Synthesis of Programmable Reaction-Diffusion Fronts Using DNA Catalyzers

Anton S. Zadorin,[1] Yannick Rondelez,[2] Jean-Christophe Galas,[1] and André Estevez-Torres[1,*]
[1]*Laboratoire de photonique et de nanostructures, CNRS, route de Nozay, 91460 Marcoussis, France*
[2]*LIMMS/CNRS-IIS, University of Tokyo, Komaba, 4-6-2 Meguro-ku, Tokyo, Japan*
(Received 6 October 2014; published 9 February 2015)

We introduce a DNA-based reaction-diffusion (RD) system in which reaction and diffusion terms can be precisely and independently controlled. The effective diffusion coefficient of an individual reaction component, as we demonstrate on a traveling wave, can be reduced up to 2.7-fold using a self-assembled hydrodynamic drag. The intrinsic programmability of this RD system allows us to engineer, for the first time, orthogonal autocatalysts that counterpropagate with minimal interaction. Our results are in excellent quantitative agreement with predictions of the Fisher-Kolmogorov-Petrovskii-Piscunov model. These advances open the way for the rational engineering of pattern formation in pure chemical RD systems.

DOI: 10.1103/PhysRevLett.114.068301 PACS numbers: 82.40.Ck, 82.39.Pj, 82.40.Qt

Reaction-diffusion (RD) models are a rich source of spatiotemporal pattern formation phenomena. Not only is this mechanism relevant to biological morphogenesis [1], but it is one of the few conceptualizations that physics can offer for the spontaneous emergence of order in molecular systems [2]. Traveling waves [3], spirals [4] and Turing patterns [5], among other structures [6,7], have been observed experimentally. However, in contrast to pattern formation in hydrodynamics, few of these studies are quantitative [8,9]. The reason for this is that we lack a fully controllable and easily modeled experimental RD system. In addition, to generate arbitrary spatiotemporal patterns, the following properties need to be programmable: (i) the topology of the chemical reaction network (CRN), (ii) the reaction rates, and (iii) the diffusion coefficients of the individual species D_i. The majority of attempts to achieve these goals concern redox or acid-base reactions related to the Belousov-Zhabotinsky (BZ) reaction [10–12]. Our current understanding does not allow us to engineer CRNs with such chemistries in a rational way. Although semiheuristic methods have been developed [13–15], they are neither general nor modular. Particular solutions to control diffusion have been devised for BZ-related reactions [5,16], but no general strategy is available.

DNA-based chemical reaction networks provide an interesting solution to the issues mentioned above. Because of base complementarity, the kinetics of the DNA hybridization reaction can be predicted from the sequence [17,18]. Recent advances in DNA nanotechnology allow us to program the topology of quite complex CRNs. Enzyme-free DNA circuits have been used for producing tunable cascading reactions [19] and encoding edge detection algorithms [20]. In combination with enzymatic reactions, nonequilibrium dissipative behaviors with DNA circuits have been obtained, such as nonlinear oscillators [21–23], memory switches [24], and propagating waves and spirals [25].

Here we introduce a general method to specifically control the reaction and diffusion rates of the DNA species involved in such programmable reaction networks. We demonstrate this on the minimal reaction capable of self-organization in space: an autocatalytic front propagating in a one-dimensional reactor. As such, we used an autocatalytic node of the DNA polymerase exonuclease nicking enzyme (PEN) toolbox, which works as follows [21]. Species A, an 11-mer single-stranded DNA, catalyzes its own growth in the presence of a template strand T, a 22-mer that carries two contiguous domains complementary to A: species A reversibly hybridizes with T on either of these domains and one of the resulting complexes can be extended by a polymerase, which is the rate-limiting step in our conditions. The resulting double-stranded DNA complex carries a recognition site for a nicking enzyme (nick) such that the upper strand is cut at its midpoint, releasing two molecules of A and the intact T. The kinetics of this process is captured by the simplified mechanism sketched in Fig. 1(a) (for details refer to Refs. [21,25]). The total concentration of each species, free or bound, is noted in italics in the following.

In a one-dimensional reactor the evolution of A is described by the reaction-diffusion equation

$$\frac{\partial A}{\partial t} = r(A) + \frac{\partial}{\partial x}\left(D_{\mathrm{eff}}(A)\frac{\partial A}{\partial x}\right), \tag{1}$$

where $r(A)$ is the reaction term, and we have made explicit that the effective diffusion coefficient $D_{\mathrm{eff}}(A)$ depends on A. This reflects the existence of A in states with different diffusion coefficients (free and bound to T). When $D_{\mathrm{eff}}(A) = D$, Eq. (1), together with reasonable assumptions about $r(A)$ [26], forms the Fisher-Kolmogorov-Petrovskii-Piscunov (FKPP) case: there exists a single stable asymptotic traveling wave solution $A(x,t) = A(x - v_m t)$, where $v_m = 2\sqrt{r'(0)D}$ depends neither on

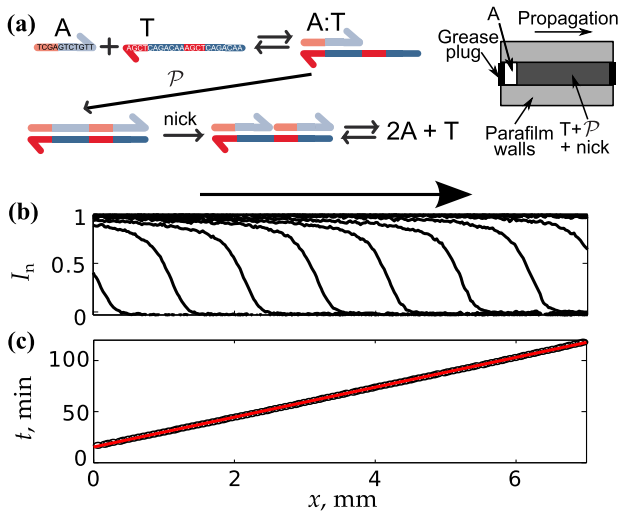

FIG. 1 (color online). A DNA-based autocatalyst generates a front traveling with uniform velocity in a channel reactor. (a) Simplified mechanism of the autocatalytic growth of A on T (left) and sketch of the experimental setup (right). (b) Experimental profiles of normalized fluorescence intensity I_n along the channel length, x, in 15 min intervals. The arrow shows the direction of propagation. (c) Time vs the position of the front (linear fit in red). $T_0 = 200\,\mathrm{n}M$, 38 °C.

other details of the growth function $r(A)$ nor on the shape of the initial condition [27,28]. In our case, if the front propagation is controlled by the growth at the leading edge, where $A \simeq 0$, we can assume [29]

$$D = D_{\mathrm{eff}}(0) \approx \frac{K}{2T_0 + K} D_{\mathrm{A}} + \frac{2T_0}{2T_0 + K} D_{\mathrm{A:T}}, \qquad (2)$$

where K is the dissociation constant of A with its complementary sequence in T, T_0 the total concentration of T, and D_{A} and D_{T} the diffusion coefficients of free A and free T, respectively. In the following we approximate $D_{\mathrm{A:T}}$ by D_{T}. We thus have,

$$v_m = 2\sqrt{r'(0) D_{\mathrm{eff}}(0)}. \qquad (3)$$

To take into account deviations between our experiments and the model described above, we introduce a phenomenological correction factor γ such that $v = \gamma v_m$, where v is the experimentally measured velocity and v_m is given by Eqs. (2) and (3). We hypothesize that γ results from considering the complex growth of A (involving several DNA hybridization and enzymatic reactions) as a single step A → 2A with a single average species A. We will demonstrate that our programmable molecular system is in quantitative agreement with the model when $\gamma = 1.3$.

In our experiments, A was indirectly monitored using the nonspecific fluorescent DNA binder EvaGreen. An elongated channel (2 cm × 2 mm × 200 μm) was fabricated by thermally bonding a precut Parafilm sheet between two polystyrene slides [Fig. 1(a)]. The channel was first filled with a solution containing all components (T, enzymes, and deoxyribonucleotides) except A. Subsequently, 1 μM of A was injected into the left inlet using a micropipette [30]. After sealing the two ends to prevent evaporation and hydrodynamic flow, the fluorescence intensity in the channel was recorded using a microscope equipped with a 2.5× objective and a CCD camera. We observed a front of fluorescence that moved from left to right [Figs. 1(b) and 1(c)]. The shape of the intensity profile along x was stable in time. The front propagated at a constant velocity of 65 ± 5 μm/ min for about 150 min before reaching the right end of the channel. The observed velocity did not depend on the injection step or on the injected concentration of A, in agreement with the FKPP case. In a set of independent experiments we measured $r'(0)$, D_{A}, D_{T}, and K. We measured $r'(0) = 0.077 \pm 0.013\ \mathrm{min}^{-1}$ by recording the fluorescence intensity as a function of time, which was exponential at short times (and low A), in a well-mixed reactor [31]. We measured $D_{\mathrm{A}} = (16 \pm 3) \times 10^3\ \mu\mathrm{m}^2/\mathrm{min}$ and $D_{\mathrm{T}} = (10.7 \pm 0.7) \times 10^3\ \mu\mathrm{m}^2/\mathrm{min}$ at 38 °C from the relaxation of a sharp initial concentration profile. As an approximation for K we measured the dissociation constant of the hybridization of A with its complementary strand and found $K = 3$ nM at 38 °C. From Eqs. (2) and (3) our model predicts $v_m = 59 \pm 7$ μm/ min, which is just 10% below the experimental value ($\gamma = v/v_m = 1.1 \pm 0.2$).

To check the scaling $v \sim [r'(0)]^{1/2}$ and the capability of the model to provide a quantitative prediction of v with a unique value of γ, we measured $r'(0)$ and v for different T_0 and $\mathcal{P}$ (where $\mathcal{P}$ is the polymerase concentration) (Fig. 2, Ref. [32]). Figures 2(a) and 2(b) show the dependence on T_0. The growth of the autocatalyst was always exponential at short times, with a linear dependence, $r'(0) = (3.1 \times 10^{-4}\ \mathrm{n}M^{-1}\,\mathrm{min}^{-1}) \times T_0$, in the range $T_0 = 0$–100 nM. The growth rate can thus be specifically tuned by changing T_0—an important feature for modular programmability [Fig. 2(a)]. The velocity of the front also depended on T_0. Fronts propagated faster as T_0 increased. Since we found $r'(0) \sim T_0$, Eq. (3) predicted that $v^2 \sim T_0$, which was verified experimentally for $T_0 = 0$–200 nM. We used the values of D_i, K, and $r'(0)$ reported above to calculate v_m with Eqs. (2) and (3), resulting in $\gamma = 1.30 \pm 0.16$, in agreement with the value reported above. With $\gamma = 1.3$, Eq. (3) is in excellent agreement with the data [Fig. 2(b), blue line]. Note that A in the back of the front increased with T_0. The good agreement between the model and the experiment in Fig. 2(b) thus supports our approximation $D_{\mathrm{eff}}(A) \approx D_{\mathrm{eff}}(0)$.

Control experiments showed that the reaction rate was limited by the polymerization step rather than by the subsequent cleavage by the nickase. We thus expected $r'(0) \sim \mathcal{P}$ which gave us another opportunity to verify the validity of the scaling predicted by the FKPP model. As a

test of the robustness of the model's predictions, we verified this scaling at a different temperature, 44 °C, and nicking enzyme concentration, 500 U/ml [Figs. 2(c) and 2(d)]. $r'(0)$ linearly depended on $\mathcal{P}$, with $r'(0) = (0.05\ \mathrm{min}^{-1}) \times \mathcal{P}_n$ in the range $\mathcal{P}_n = 0$–2. In the range $\mathcal{P}_n = 0$–1, $v^2 \sim \mathcal{P}_n$, and the velocities predicted by Eqs. (2) and (3) with $\gamma = 1.3$ were, again, in excellent agreement with the experimental ones [Fig. 2(d), blue line] [33]. Only for $\mathcal{P}_n = 2$ was v underestimated by the model. We speculate that this nonlinear effect may come from a transition from a pulled [FKPP, $r'(A) \leq r'(0)$] to a pushed front [$r'(A) > r'(0)$] [34].

In addition to controlling reaction rates, the ability to change diffusion coefficients is essential for pattern formation. For instance, no Turing bifurcation is possible with equal diffusion coefficients in a homogeneous system [10]. The validity of Eq. (3) provides an experimental way to measure changes in $D_{\mathrm{eff}}(0)$ and thus monitor our capacity for controlling diffusion. Tuning the diffusion coefficient, D, of a molecule is not a simple task. Indeed, for a random coil, $D \sim M^{-1/2}$, where M is the molecular mass. As a result, to reduce D significantly, relatively large molecular entities are needed. However, these entities need not necessarily be covalent or even stable: if A interacts dynamically with a ligand, its effective diffusion coefficient $D_{\mathrm{eff}}(0)$ will be a weighted average between the free state with high D and the bound state with low D, as illustrated in Eq. (2). This approach applies well to single-stranded DNA species, for which a binding partner always exists as its Watson-Crick complementary. The task then breaks down to reducing the diffusion of that partner.

The strategy chosen here consists of attaching a hydrodynamic drag to the 3′ end of template T, which binds to the active species A. We used a T modified with a hydrophobic cholesteryl group in 3′ (which we note as T-ch) in a 10 g/l triton X-100 solution. At this concentration this surfactant forms micelles about 5.5 nm in radius [35]. The cholesteryl group is expected to reversibly attach to them through hydrophobic interactions and form species T-ch:trit, with lower diffusion.

Figure 3(a) shows the propagation of a front of A growing on either T or T-ch in a triton solution with the same reaction conditions [36]. The second front advances 1.6 ± 0.2 times slower, the velocities being 65 ± 5 and $40 \pm 4\ \mu\mathrm{m/min}$, respectively (confidence level 0.95). In contrast, the influence of the triton drag on the growth kinetics appeared to be negligible. We measured $r'(0) = 0.078 \pm 0.005\ \mathrm{min}^{-1}$ for T-ch:trit, which is identical, within experimental error, to the growth rate for T [37]. These values, according to Eq. (3), give $D_{\mathrm{eff}}(0) = (5.1 \pm 1.1) \times 10^3\ \mu\mathrm{m}^2/\mathrm{min}$, corresponding to a (2.7 ± 0.8)-fold reduction in the diffusion coefficient of the propagating species. To compare them with the prediction given by Eq. (2), we independently measured the diffusion coefficient of T-ch:trit and obtained $D_{\text{T-ch:trit}} = (4.0 \pm 0.3) \times 10^3\ \mu\mathrm{m}^2/\mathrm{min}$. Supposing that the hybridization constant is not affected by the presence of triton and thus taking $K = 3$ nM, together with $\gamma = 1.3$, the predicted velocity

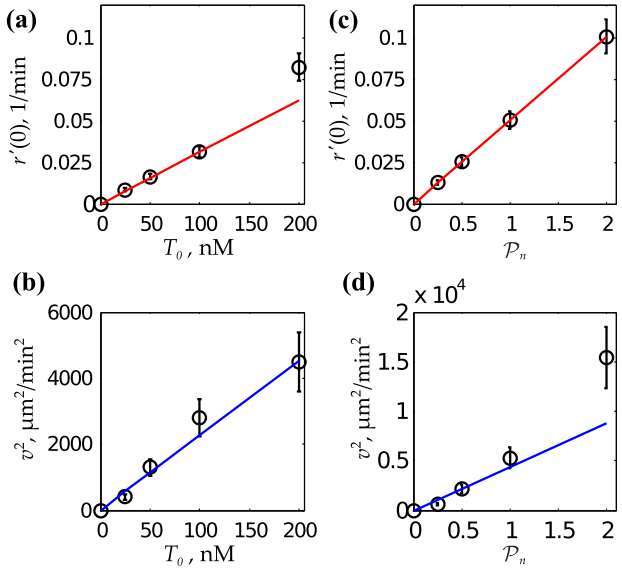

FIG. 2 (color online). The growth rate of the autocatalyst, $r'(0)$, (a), (c) and its propagation velocity, v, (b), (d) can be tuned specifically with the template concentration, T_0, and nonspecifically with the normalized polymerase concentration, $\mathcal{P}_n$. The red line is a linear fit for $T_0 = 0$–100 nM (a) and $\mathcal{P}_n = 0$–2. Blue lines are predictions using Eqs. (2) and (3) with $\gamma = 1.3$. Experimental conditions (a),(b) 38 °C, (c),(d) 44 °C. $\mathcal{P}_n = \mathcal{P}/(16\ \mathrm{U/ml})$. Error bars for $r'(0)$ and v were estimated from four independent experiments at $T_0 = 200$ nM.

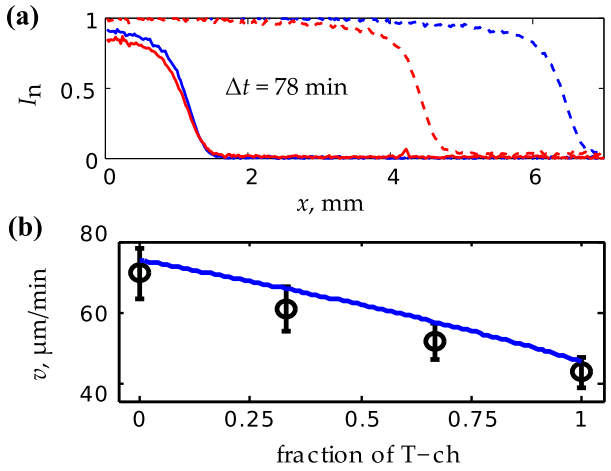

FIG. 3 (color online). The diffusion coefficient of the propagating species can be finely tuned using a hydrodynamic drag. (a) Fluorescence profiles of propagating fronts generated by T:trit (blue lines) and T-ch:trit (red lines) in different channels, at $t = 0$ min (solid lines) and $t = 78$ min (dashed lines). (b) Fine-tuning of the front velocity through diffusion by changing the molar fraction of T-ch compared to T and keeping $T_0 + T\text{-ch}_0 = 200$ nM constant, the line is the theoretical prediction from Eqs. (2) and (3) with $\gamma = 1.3$. 10 g/l triton X-100, 38 °C.

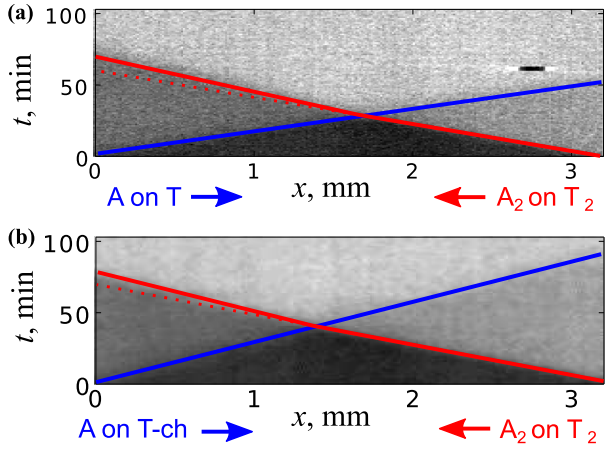

FIG. 4 (color online). Two independent autocatalysts counterpropagate with minimal interaction. Kymographs (time vs position) for a front of A (blue lines), propagating from left to right, and a front of A_2 (red lines), propagating from right to left. (a) A grows on T. (b) A grows on T-ch:trit. Dark, semibright, and bright areas correspond to spaces with 0, 1, and 2 propagating fronts, respectively. Lines are visual guides to show the position of the front, with dashed ones indicating a constant velocity of A_2. $T_0 = T\text{-ch}_0 = T_{2,0} = 150$ nM, 10 g/l of triton X-100, 38 °C.

for the front based on T-ch is 46 ± 2 μm/ min and the theoretical expectation of the change of $D_{\mathrm{eff}}(0)$ in the presence of a drag is (2.6 ± 0.2)-fold. In addition, in a channel containing both T and T-ch:trit, we achieved fine tuning of the velocity of a front of A by varying the molar fraction of T-ch:trit while keeping the total concentration (T + T-ch : trit) constant [Fig. 3(b)]. The theoretical prediction [Eqs. (2) and (3)] with the phenomenological correction $\gamma = 1.3$ was, in all of these experiments, in excellent agreement with the experimental data without fitting, indicating that the diffusion coefficient of a propagating autocatalyst can be tuned in a quantitative manner.

Finally, to demonstrate the potential of our approach to run different noninteracting modules in the same reactor, we designed a second autocatalyst orthogonal to A: A_2 produced by the template T_2. A_2 had a different base at every sequence position of its template and depended on a different nicking enzyme. Its growth was slightly faster: $r'(0) = 0.13$ min^{-1} for $T_{2,0} = 200$ nM. In a channel containing a mix of T and T_2, two fronts propagating in opposite directions could be triggered by injecting A and A_2 on the left and right inlets, respectively (Fig. 4(a) and Ref. [38]). For $T_0 = T_{2,0} = 150$ nM; at $t < 32$ min, each front propagated in a fresh medium and they each behaved as an independent front, as expected. When the two fronts encountered each other, A maintained its velocity constant, which was equal to 54 μm/ min, while the velocity of A_2 was reduced 1.3-fold from 48 to 37 μm/ min. The minimal interaction between the two fronts is particularly striking. It results from the fact that A and A_2 grow on quasi-independent resources; the slight interaction coming from them sharing polymerase. This situation is very different from classic BZ systems where two colliding fronts annihilate each other because they need the same chemicals to grow. To the best of our knowledge, this is the first time that the counterpropagation of two chemically distinct fronts has been observed. In this configuration, substituting T by T-ch allowed us to specifically control the effective diffusion coefficient of A, given by Eq. (2), without perturbing that of A_2 [Fig. 4(b)]. The velocity of A growing on T-ch:trit was 32 μm/ min before and after the encounter, which corresponds, again, to a velocity reduction factor of 1.7 due to the drag. The velocities of A_2 before and after the encounter were the same as reported above.

The modularity of the PEN DNA toolbox hence allows to simply design *de novo* autocatalysts from which spatiotemporal behavior can be quantitatively predicted. Beyond its striking programmability, the system presented here is commercially available and does not require particular skills in biochemistry. For these reasons, we believe that it will be widely used to investigate fascinating questions about the emergence of spatiotemporal molecular order [39].

This research was supported by ANR Jeunes Chercheurs under the Dynano grant. A. S. Z. acknowledges a postdoctoral fellowship from NanoSciences Ile-de-France (Enginets grant) and from the Laboratoire d'Excellence en Nanoscience et Nanotechnologie Nanosaclay (Turnano grant). We thank A. Kalley and M. Cabon for conducting preliminary experiments. We are indebted to L. Jullien, C. Gosse, and T. Le Saux (ENS, Paris), from whom the idea of diffusion control arose, and to D. Baigl (ENS, Paris) for the fruitful discussions.

*aestevez@lpn.cnrs.fr

[1] S. Kondo and T. Miura, Reaction-diffusion model as a framework for understanding biological pattern formation, Science **329**, 1616 (2010).
[2] M. C. Cross and P. C. Hohenberg, Pattern formation outside of equilibrium, Rev. Mod. Phys. **65**, 851 (1993).
[3] A. N. Zaikin and A. M. Zhabotinsky, Concentration wave propagation in two-dimensional liquid-phase self-oscillating system, Nature (London) **225**, 535 (1970).
[4] A. T. Winfree, Spiral waves of chemical activity, Science **175**, 634 (1972).
[5] V. Castets, E. Dulos, J. Boissonade, and P. De Kepper, Experimental Evidence of a Sustained Standing Turing-Type Nonequilibrium Chemical Pattern, Phys. Rev. Lett. **64**, 2953 (1990).
[6] K.-J. Lee, W. D. McCormick, J. E. Pearson, and H. L. Swinney, Experimental observation of self-replicating spots in a reaction–diffusion system, Nature (London) **369**, 215 (1994).
[7] V. K. Vanag and I. R. Epstein, Pattern formation mechanisms in reaction-diffusion systems, Int. J. Dev. Biol. **53**, 673 (2009).

[8] R. J. Field and R. M. Noyes, Oscillations in chemical systems. V. Quantitative explanation of band migration in the Belousov-Zhabotinskii reaction, J. Am. Chem. Soc. **96**, 2001 (1974).
[9] A. Hanna, A. Saul, and K. Showalter, Detailed studies of propagating fronts in the iodate oxidation of arsenous acid, J. Am. Chem. Soc. **104**, 3838 (1982).
[10] I. Epstein and J. A. Pojman, *An Introduction to Nonlinear Chemical Reactions* (Oxford University Press, New York, 1998).
[11] F. Sagues and I. R. Epstein, Nonlinear chemical dynamics, J. Chem. Soc. Dalton Trans. **2003**, 1201 (2003).
[12] V. K. Vanag and I. R. Epstein, Design and control of patterns in reaction-diffusion systems, Chaos **18**, 026107 (2008).
[13] J. Boissonade and P. De Kepper, Transitions from bistability to limit cycle oscillations. Theoretical analysis and experimental evidence in an open chemical system, J. Phys. Chem. **84**, 501 (1980).
[14] P. De Kepper, I. R. Epstein, K. Kustin, and M. Orban, Systematic design of chemical oscillators. Part 8. Batch oscillations and spatial wave patterns in chlorite oscillating systems, J. Phys. Chem. **86**, 170 (1982).
[15] J. Horvath, I. Szalai, and P. De Kepper, An experimental design method leading to chemical turing patterns, Science **324**, 772 (2009).
[16] V. K. Vanag and I. R. Epstein, Inwardly rotating spiral waves in a reaction-diffusion system, Science **294**, 835 (2001).
[17] M. Zuker, Mfold web server for nucleic acid folding and hybridization prediction, Nucleic Acids Res. **31**, 3406 (2003).
[18] D. Y. Zhang and E. Winfree, Control of DNA strand displacement kinetics using toehold exchange, J. Am. Chem. Soc. **131**, 17303 (2009).
[19] L. Qian and E. Winfree, Scaling up digital circuit computation with DNA strand displacement cascades, Science **332**, 1196 (2011).
[20] S. M. Chirieleison, P. B. Allen, Z. B. Simpson, A. D. Ellington, and X. Chen, Pattern transformation with DNA circuits, Nat. Chem. **5**, 1000 (2013).
[21] K. Montagne, R. Plasson, Y. Sakai, T. Fujii, and Y. Rondelez, Programming an in vitro DNA oscillator using a molecular networking strategy, Mol. Syst. Biol. **7**, 466 (2011).
[22] J. Kim and E. Winfree, Synthetic in vitro transcriptional oscillators, Mol. Syst. Biol. **7**, 465 (2011).
[23] T. Fujii and Y. Rondelez, Predator-prey molecular ecosystems, ACS Nano **7**, 27 (2013).
[24] A. Padirac, T. Fujii, and Y. Rondelez, Bottom-up construction of in vitro switchable memories, Proc. Natl. Acad. Sci. U.S.A. **109**, E3212 (2012).
[25] A. Padirac, T. Fujii, A. Estévez-Torres, and Y. Rondelez, Spatial waves in synthetic biochemical networks, J. Am. Chem. Soc. **135**, 14586 (2013).
[26] (a) Bounded growth, i.e., there exists $A_{\max} > 0$ such that $r(A_{\max}) = 0$, (b) $r(0) = 0$, (c) $r'(0) > 0$, and on $(0, A_{\max})$ (d) $r(A) > 0$, (f) $r'(A) < r'(0)$.
[27] A. Kolmogoroff, I. Petrovsky, and N. Piscounoff, Etude d'équation de la diffusion avec croissance de la quantité de matière et son application à un problem biologique, Bull. Univ. Moskou, Ser. Int., Sect. A **6**, 1 (1937) [Study of the diffusion equation with growth of the quantity of matter and its application to a biology problem, Dynamics of Curved Fronts **6**, 105 (1989)].
[28] D. G. Aronson and H. F. Weinberger, Nonlinear diffusion in population genetics, combustion, and nerve pulse propagation, in *Partial Differential Equations and Related Topics* (Springer, Berlin, 1975), p. 5.
[29] See Supplemental Material at http://link.aps.org/supplemental/10.1103/PhysRevLett.114.068301 for the derivation of Eq. (2).
[30] See Supplemental Material at http://link.aps.org/supplemental/10.1103/PhysRevLett.114.068301 for additional methods.
[31] See Supplemental Material at http://link.aps.org/supplemental/10.1103/PhysRevLett.114.068301 for Fig. S2.
[32] See Supplemental Material at http://link.aps.org/supplemental/10.1103/PhysRevLett.114.068301 for videos S1 and S2.
[33] In independent experiments we obtained $D_A = (18 \pm 3) \times 10^3\ \mu m^2/\text{min}$, $D_T = (11.8 \pm 0.8) \times 10^3\ \mu m^2/\text{min}$, and $K = 100$ nM at 44 °C.
[34] W. van Saarloos, Front propagation into unstable states, Phys. Rep. **386**, 29 (2003).
[35] H. H. Paradies, Shape and size of a nonionic surfactant micelle. Triton X-100 in aqueous solution, J. Phys. Chem. **84**, 599 (1980).
[36] See Supplemental Material at http://link.aps.org/supplemental/10.1103/PhysRevLett.114.068301 for video S3.
[37] Control measurements of enzymatic activity demonstrated that for both templates the polymerization rates were identical, while nicking rates differed by a factor of 3. Considering that polymerization is the rate-limiting step, these data demonstrate that the triton drag modifies diffusion while having a negligible influence on the growth kinetics.
[38] See Supplemental Material at http://link.aps.org/supplemental/10.1103/PhysRevLett.114.068301 for video S4.
[39] D. Scalise and R. Schulman, Designing modular reaction-diffusion programs for complex pattern formation, Technology **02**, 55 (2014).